Preprints of the 20th World Congress
The International Federation of Automatic Control
Toulouse, France, July 9-14, 2017

Induction in Optimal Control of Multiple-Kite Airborne Wind Energy Systems

Rachel Leuthold * **Sébastien Gros** ** **Moritz Diehl** *

* *Systems Control and Optimization Laboratory, Dept. of Microsystems Engineering & Dept. of Mathematics, University of Freiburg, Germany (email: rachel.colette.leuthold@imtek.uni-freiburg.de, moritz.diehl@imtek.uni-freiburg.de*
** *Department of Signals and System, Chalmers University, Sweden; Freiburg Institute for Advanced Studies, Germany (email: grosse@chalmers.se)*

Abstract: Multiple-kite Airborne Wind Energy Systems (MAWES) aim to decrease intermittency and cost over conventional wind turbines, while generating more power than other airborne wind energy systems. The purpose of this work is to estimate whether axial and angular induction are relevant phenomena in the modelling of pumping-cycle MAWES with two or more kites. Considering the modelling assumptions, axial induction is a relevant phenomenon and leads to significant changes in design-point, especially with respect to kite mass and secondary tether length. However, angular induction can be neglected in modelling for optimal design and control problems.

Keywords: airborne wind energy, induction, blade-element momentum method, power generation, windmills, optimum, model reduction, systems design

1. INTRODUCTION

Airborne Wind Energy Systems (AWES) aim to decrease both the intermittency and cost of wind energy by flying tethered aircraft, called *kites*, higher than conventional wind turbines, in *cross-wind* manoeuvres designed to maximize the kite's apparent velocity. Typically, AWES generate power either in *lift-mode* with *pumping cycle* trajectories that wind and unwind a ground-station generator, or in *drag-mode* with onboard power production. (Loyd, 1980)

For single-kite AWES, tether drag can be significant, as the top of the tether perceives the same high apparent velocities as the kite. This is unfortunate, as the total available power for an AWES is inversely proportional to the square of the system drag. A *Multiple-kite AWES* (MAWES) (see Figure 1) reduces tether drag over a single-kite AWES by splitting the main tether into two or more secondary tethers, each holding an equivalent kite. As the main tether does not travel cross-wind, the total tether drag for a MAWES is less than for a single-kite AWES.

Like all wind energy systems, MAWES convert the flow kinetic energy into electrical energy. The kinetic energy decrease of an incompressible fluid occurs gradually, such that the flow arrives at the kite location with a slower velocity than the free-stream. This phenomenon, called *induction*, decreases the available energy within the flow

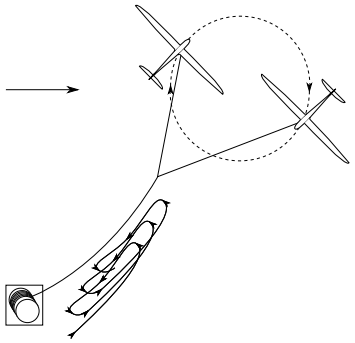

Fig. 1. A sketch of a two-kite ($N = 2$) MAWES

along the *axial*, *angular*, and *radial* coordinates of MAWES kite rotation. For model parsimony in optimal design and control of MAWES, it should be determined whether induction can be safely neglected in MAWES models.

This is not a trivial question, given that induction has widely different levels of influence in similar systems. For single-kite drag-mode AWES, Vander Lind (2014) reports that induction has no practical effect because crosswind velocity dominates the kite's apparent velocity. As a result, current studies of MAWES (Houska and Diehl, 2007; Zanon et al., 2013) typically neglect induction. However, induction is well established to have a large impact (Manwell et al., 2009) on horizontal axis wind turbines. Further, Zanon et al. (2014) estimates that axial induction can decrease available power in a two-kite drag-mode MAWES by 39 percent.

⋆ Support by the EU via ERC-HIGHWIND (259 166), ITN-TEMPO (607 957), and ITN-AWESCO (642 682) and by DFG in context of the Research Unit FOR 2401 is gratefully acknowledged.

As far as the authors are aware, induction effects in MAWES of more than two kites, especially considering angular induction and lift-mode power generation, have not yet been studied. Consequently, the purpose of this work is to assess whether it is necessary to include axial and angular induction in the modelling of a lift-mode MAWES with two or more kites. Radial induction is outside the scope of this analysis.

The approach chosen here is to maximize the power output of a highly-idealized lift-mode MAWES, and consider whether induction strongly changes the optimization result, in terms of performance and design. Induction effects can be modelled using the Blade-Element Momentum method (BEM) (Manwell et al., 2009), to include either *No Induction* (NI), *only Axial Induction* (AI) or *Axial and Angular induction* (AA), by selectively requiring that the net downwind force and torque equal the flow downwind momentum change.

2. ASSUMPTIONS FOR A HIGHLY-IDEALIZED MAWES PROBLEM

Under certain assumptions, the MAWES problem simplifies significantly into a highly-idealized MAWES problem. First, for cross-wind flight at large angular velocities, gravitational forces may be negligible in the face of kite centrifugal and aerodynamic forces. Second, the wind shear may be negligible, if the secondary tethers are much shorter than the main tether. By also neglecting atmospheric turbulence, the free-stream wind field is rendered approximately uniform. Further, when the gravitational and drag force on the main tether are much smaller than the total force acting on the system, the main tether might be neglected entirely.

Under these assumptions, the MAWES problem becomes axisymmetric and rotationally-steady about the free-stream wind direction. Then, an analysis of one kite-and-secondary-tether describes the entire MAWES. Rotational-steadiness requires that the forces from this kite-and-tether be parallel to the secondary tether. However, as the tethers are modelled rigidly and the forces acting on the kite-and-secondary tether are not applied at the same location, the torque from the modelled forces may be nonzero. To ensure that the net torque is still zero and satisfies rotational-steadiness, it is assumed that there is a balancing pure-moment acting at the tether connection point.

The kite of the single kite-and-secondary-tether within this static problem is approximated as a thin, symmetric, and elliptical wing, with some mean aerodynamic chord c, span b, and mass m. As it is assumed that there is a vertical stabilizer to generate restoring yaw momentum, the elliptical wing is oriented not to experience side-slip. Additionally, the angle-of-attack (AoA) must be small such that the flow remains attached. The secondary tether is assumed to be straight - without sag or strain, and with a uniform diameter ϕ and density ρ_T - and attached to the kite's center of gravity.

Then, a MAWES can be highly-idealized (see Figure 2) as a N-symmetric system, using a symmetric coordinate system with axial $\hat{\boldsymbol{x}}$, tangential $\hat{\boldsymbol{y}}$, and radial $\hat{\boldsymbol{z}}$ basis vectors. The kite is oriented with chord-wise $\hat{\boldsymbol{e}}_1$, span-wise $\hat{\boldsymbol{e}}_2$, and up $\hat{\boldsymbol{e}}_3$ basis vectors.

The problem is non-dimensionalized for design-point comparison and numerical conditioning. Non-dimensionalization is indicated with a "tilde" such that the free-stream velocity vector $\boldsymbol{U}_\infty = U_\infty \hat{\boldsymbol{x}}$ can be described as $\widetilde{\mathbf{U}}_\infty = \hat{\boldsymbol{x}}$.

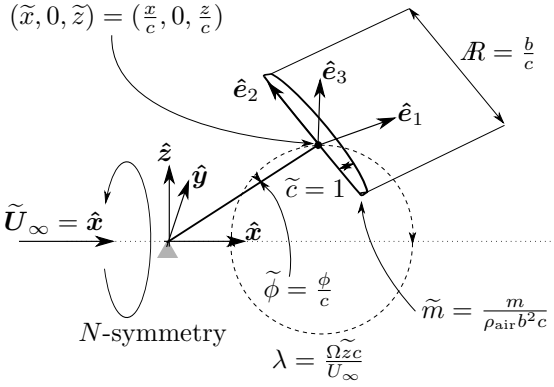

Fig. 2. Parameters in a highly-idealized MAWES

The equivalent kite has its center of gravity at $(\widetilde{x}, 0, \widetilde{z}) = (x/c, 0, z/c)$ and is described by a normalized mean aerodynamic chord $\widetilde{c} = 1$, aspect ratio $\mathcal{R} = b/c$, and tether diameter ratio $\widetilde{\phi} = \phi/c$. To prevent collisions, it is assumed that $\widetilde{z}$ must be greater than or equal to half of the aspect ratio $\mathcal{R}$:

$$\widetilde{z} - \tfrac{1}{2}\mathcal{R} \geq 0. \tag{1}$$

The mass of the kite is described by a mass-ratio $\widetilde{m} = m/(\rho_{\text{air}} b^2 c)$ that increases with both the planform area and the span, due to additional internal stiffening. The angular velocity Ω sets the tip-speed-ratio $\lambda = \Omega \widetilde{z} c / U_\infty$; the reel-out velocity $f U_\infty \hat{\boldsymbol{x}}$ sets the reel-out factor f.

3. THE BLADE-ELEMENT MOMENTUM METHOD

The BEM can be applied to the above idealized MAWES, beginning with a definition of the axial a and angular a' induction factors:

$$a = 1 - \widetilde{u}_{\text{w}} = 1 - \frac{u_{\text{w}}}{U_\infty}, \tag{2}$$

$$a' = \frac{\widetilde{v}_{\text{w}}}{\lambda} = \frac{1}{\lambda}\frac{v_{\text{w}}}{U_\infty} = \frac{\omega}{\Omega}, \tag{3}$$

where the flow velocity at the kite location is considered to be $\boldsymbol{u}_{\text{w}} = u_{\text{w}}\hat{\boldsymbol{x}} + v_{\text{w}}\hat{\boldsymbol{y}} = U_\infty(\widetilde{u}_{\text{w}}\hat{\boldsymbol{x}} + \widetilde{v}_{\text{w}}\hat{\boldsymbol{y}})$, and ω is the angular induced velocity.

In BEM, thrust and torque expressions are implicit functions of the two induction factors. The thrust can be non-dimensionalized by the free-stream dynamic pressure $q_\infty = \frac{1}{2}\rho_{\text{air}} U_\infty^2$, and the kite planform area $S = bc$. The torque is additionally non-dimensionalized by the mean aerodynamic chord c:

$$\widetilde{T} = \frac{T}{q_\infty S} = N\,\frac{\boldsymbol{F}\cdot\hat{\boldsymbol{x}}}{q_\infty S} = N\,\widetilde{\mathbf{F}}\cdot\hat{\boldsymbol{x}}, \tag{4}$$

$$\widetilde{Q} = \frac{Q}{q_\infty S c} = N\,\frac{\boldsymbol{Q}\cdot(-\hat{\boldsymbol{x}})}{q_\infty S c} = N\,\widetilde{\mathbf{Q}}\cdot(-\hat{\boldsymbol{x}}), \tag{5}$$

where T is the thrust, $\boldsymbol{F}$ the total force on the individual kite, Q the torque component along the axis of rotation for flow counter-clockwise rotation when facing downstream, and $\boldsymbol{Q}$ the total torque vector.

Consequently, the inclusion of induction into the BEM aerodynamic model depends on the thrust and torque expressions of both the blade-element- and momentum-perspectives.

3.1 Blade-Element Thrust and Torque Expressions

In comparison to the standard blade-element perspective, it may be reasonable to trade the complexity of spanwise blade discretization with empirical tip-loss corrections, for three-dimensional potential-flow aerodynamic coefficient approximations. This is because a MAWES kite-and-secondary-tether likely has less spanwise apparent velocity variation but more significant tip losses than a wind turbine blade.

Consequently, the thrust and torque from the blade-element perspective depend on summing all of the forces and moments on the the kite-and-secondary-tether.

Kite Forces and Moments The kite's contribution to the force and moment balance considers lift, drag, and centrifugal forces.

The aerodynamic kite forces depend on the apparent velocity $\widetilde{\mathbf{u}}_\mathrm{a}$, determined from the wind velocity at the kite location $\widetilde{\mathbf{u}}_\mathrm{w}$ and the kite's velocity $\widetilde{\mathbf{u}}_\mathrm{k}$:

$$\widetilde{\mathbf{u}}_\mathrm{w} = (1-a)\hat{\boldsymbol{x}} + a'\lambda\hat{\boldsymbol{y}} \tag{6}$$
$$\widetilde{\mathbf{u}}_\mathrm{k} = f\hat{\boldsymbol{x}} - \lambda\hat{\boldsymbol{y}} \tag{7}$$
$$\widetilde{\mathbf{u}}_\mathrm{a} = \widetilde{\mathbf{u}}_\mathrm{w} - \widetilde{\mathbf{u}}_\mathrm{k} \tag{8}$$

Without side-slip, the apparent velocity is in the $\hat{\boldsymbol{e}}_1$, $\hat{\boldsymbol{e}}_3$ plane. Then, introducing ξ, $\zeta \in \mathbb{R}$, the following holds:

$$\widetilde{\mathbf{u}}_\mathrm{a} - (\xi\hat{\boldsymbol{e}}_1 + \zeta\hat{\boldsymbol{e}}_3) = \mathbf{0}. \tag{9}$$

The variables ξ and ζ yield a simple expression for the AoA ($\alpha = \arctan(\zeta/\xi) \approx \zeta/\xi$), which must remain between $\alpha_\mathrm{min} = -12^o$ and $\alpha_\mathrm{max} = 12^o$, for fully-attached flow (Jacobs and Sherman, 1937). Then, the following holds:

$$\zeta - \xi\alpha_\mathrm{min} \geq 0, \quad \text{and} \quad \xi\alpha_\mathrm{max} - \zeta \geq 0. \tag{10}$$

To ensure that the direct cosine matrix $\mathbf{R} = (\hat{\boldsymbol{e}}_1, \hat{\boldsymbol{e}}_2, \hat{\boldsymbol{e}}_3)$ is a rotation matrix, it is required that:

$$\mathcal{P}\left(\mathbf{R}^T\mathbf{R} - \mathbf{I}\right) = \mathbf{0}, \tag{11}$$

where $\mathcal{P} : \mathbb{R}^{3\times3} \to \mathbb{R}^6$ is a linear projection operator that selects the upper triangular elements and ensures that the Jacobian of (11) is full rank.

From thin airfoil theory, with a streamlined aircraft's parasite drag (Von Mises, 1959) coefficient $C_{D_0} = 0.10$, the three-dimensional lift and drag coefficients read as:

$$C_L = \frac{2\pi\alpha}{1 + 2/\mathit{AR}}, \quad \text{and} \quad C_D = C_{D_0} + \frac{C_L^2}{\pi\mathit{AR}}. \tag{12}$$

Then the non-dimensional kite centrifugal $\widetilde{\mathbf{C}}$, lift $\widetilde{\mathbf{L}}$ and drag $\widetilde{\mathbf{D}}$ forces acting approximately on the center of gravity can be determined:

$$\widetilde{\mathbf{C}} = \frac{m\Omega^2 z}{q_\infty S} = 2\frac{\widetilde{m}\mathit{AR}\lambda^2}{\widetilde{z}}\hat{\boldsymbol{z}}, \tag{13}$$
$$\widetilde{\mathbf{L}} = C_L\,||\widetilde{\mathbf{u}}_\mathrm{a}||_2^2\,\frac{\widetilde{\mathbf{u}}_\mathrm{a}\times\hat{\boldsymbol{e}}_2}{||\widetilde{\mathbf{u}}_\mathrm{a}\times\hat{\boldsymbol{e}}_2||_2}, \tag{14}$$
$$\widetilde{\mathbf{D}} = C_D\,||\widetilde{\mathbf{u}}_\mathrm{a}||_2\,\widetilde{\mathbf{u}}_\mathrm{a}, \tag{15}$$

for which the torque on the tether-connection point is:

$$\widetilde{\mathbf{Q}}_\mathrm{k} = (\widetilde{x}\hat{\boldsymbol{x}} + \widetilde{z}\hat{\boldsymbol{z}}) \times \left(\widetilde{\mathbf{C}} + \widetilde{\mathbf{L}} + \widetilde{\mathbf{D}}\right). \tag{16}$$

Tether Forces and Moments The tether is assumed to experience only drag and centrifugal forces.

Integration along the straight tether determines the tether drag force $\widetilde{\mathbf{D}}_T$. This integration approximates the apparent velocity distribution as linear between a velocity-free tether-connection point and the kite $\widetilde{\mathbf{u}}_{\mathrm{a},T} = \widetilde{\mathbf{u}}_\mathrm{a}U_\infty\, l/\left(\sqrt{\widetilde{x}^2+\widetilde{z}^2}\right)$. Drag is assumed only to act on the length perpendicular to the apparent velocity, using a factor $l_\perp = \sin(\arccos((\widetilde{x}\hat{\boldsymbol{x}} + \widetilde{z}\hat{\boldsymbol{z}}) \cdot \widetilde{\mathbf{u}}_\mathrm{a}/((\sqrt{\widetilde{x}^2+\widetilde{z}^2})\,||\widetilde{\mathbf{u}}_\mathrm{a}||_2)))$, with a drag coefficient $C_{D,T} = 1.0$ (Von Mises, 1959).

$$\begin{aligned}\widetilde{\mathbf{D}}_T &= \frac{\int_0^{c\sqrt{\widetilde{x}^2+\widetilde{z}^2}} C_{D,T}\left(\frac{1}{2}\rho_\mathrm{air}\,||\boldsymbol{u}_{\mathrm{a},T}||_2\right)(\phi l_\perp dl)\,\boldsymbol{u}_{\mathrm{a},T}}{q_\infty S} \\ &= \frac{C_{D,T}}{3}\frac{||\widetilde{\mathbf{u}}_\mathrm{a}||_2\,l_\perp\widetilde{\phi}\sqrt{\widetilde{x}^2+\widetilde{z}^2}}{\mathit{AR}}\widetilde{\mathbf{u}}_\mathrm{a}.\end{aligned} \tag{17}$$

Integration also gives the tether drag torque $\widetilde{\mathbf{Q}}_{T_D}$:

$$\begin{aligned}\widetilde{\mathbf{Q}}_{T_D} &= \frac{C_{D,T}\phi l_\perp \int_0^{c\sqrt{\widetilde{x}^2+\widetilde{z}^2}}\left(\frac{1}{2}\rho_\mathrm{air}\,||\boldsymbol{u}_{\mathrm{a},T}||_2\right) l dl\,\frac{(\widetilde{x}\hat{\boldsymbol{x}}+\widetilde{z}\hat{\boldsymbol{z}})\times\boldsymbol{u}_{\mathrm{a},T}}{\left(\sqrt{\widetilde{x}^2+\widetilde{z}^2}\right)}}{q_\infty Sc} \\ &= \frac{C_{D,T}}{4}\frac{||\widetilde{\mathbf{u}}_\mathrm{a}||_2\,l_\perp\widetilde{\phi}\sqrt{\widetilde{x}^2+\widetilde{z}^2}}{\mathit{AR}}\left((\widetilde{x}\hat{\boldsymbol{x}} + \widetilde{z}\hat{\boldsymbol{z}}) \times \widetilde{\mathbf{u}}_\mathrm{a}\right).\end{aligned} \tag{18}$$

Futher, using the nondimensional tether density $\widetilde{\rho}_T = \rho_T/\rho_\mathrm{air}$, the tether centrifugal force $\widetilde{\mathbf{C}}_T$ reads as:

$$\begin{aligned}\widetilde{\mathbf{C}}_T &= \frac{\int_0^{c\sqrt{\widetilde{x}^2+\widetilde{z}^2}}\left(\rho_T\frac{\pi}{4}\phi^2 dl\right)\Omega^2\left(\frac{l\widetilde{z}\hat{\boldsymbol{z}}}{\sqrt{\widetilde{x}^2+\widetilde{z}^2}}\right)}{q_\infty S} \\ &= \frac{\pi}{4}\widetilde{\phi}^2\widetilde{\rho}_T\frac{\lambda^2}{\mathit{AR}}\frac{\sqrt{\widetilde{x}^2+\widetilde{z}^2}}{\widetilde{z}}\hat{\boldsymbol{z}}.\end{aligned} \tag{19}$$

Geometrically, the tether centrifugal torque points along negative $\hat{\boldsymbol{y}}$ and has no component in the $\hat{\boldsymbol{x}}$ direction.

The kite and tether forces and moments can now be combined to find the blade element thrust and torque expressions.

Net Thrust, Torque, and Power The previously defined forces in (13), (14), (15), (17), and (19) as well as torques (16) and (18) can be combined into resultant thrust and torque expressions that will help determine the MAWES induction. Further, the resultant thrust contributes to a power expression that can act as a figure-of-merit for a given MAWES design.

The resultant non-dimensional force per kite $\widetilde{\mathbf{F}}$ reads as:

$$\widetilde{\mathbf{F}} = \widetilde{\mathbf{C}} + \widetilde{\mathbf{L}} + \widetilde{\mathbf{D}} + \widetilde{\mathbf{C}}_T + \widetilde{\mathbf{D}}_T. \tag{20}$$

As the problem is assumed to be rotationally-steady, the resultant force must be parallel to the secondary tether. Introducing the scaling variable $\kappa \in \mathbb{R}$, the following holds:

$$\widetilde{\mathbf{F}} - \kappa\left(\widetilde{x}\hat{\boldsymbol{x}} + \widetilde{z}\hat{\boldsymbol{z}}\right) = \mathbf{0}. \tag{21}$$

Further, the stress in the tether must be less than some tolerable stress σ_T, non-dimensionalized as $\sigma_T = \widetilde{\sigma}_T\ q_\infty$:

$$\frac{\pi}{4}\widetilde{\sigma}_T\widetilde{\phi}^2 - \left|\left|\widetilde{\mathbf{F}}\right|\right|_2 \not{R} \geq 0. \tag{22}$$

The total non-dimensional torque in the $-\hat{\boldsymbol{x}}$ direction, reads as:

$$\widetilde{Q} = N\left(\widetilde{\mathbf{Q}}_\mathrm{k} + \widetilde{\mathbf{Q}}_{T_D}\right)\cdot\left(-\hat{\boldsymbol{x}}\right). \tag{23}$$

The MAWES produces power by reeling out the tether at a velocity $fU_\infty\hat{\boldsymbol{x}}$ under the total force. Using (4) and (20):

$$\widetilde{P} = \widetilde{T}f. \tag{24}$$

BEM requires a thrust and torque expression from the momentum perspective, to equate to the determined thrust and torque expression from the blade-element perspective.

3.2 Momentum Thrust and Torque Expressions

To implicitly solve for induction using BEM, momentum-perspective expression for thrust and torque are needed.

The momentum-perspective argument is based on the assumption that there is an annular streamtube, which contains the MAWES kites at an "actuator annulus", and holds potential flow in equilibrium. The flow at each annulus is assumed homogeneous. Further, it is assumed that the kite-and-secondary-tether only perform work on the flow in the actuator annulus, across which the work is distributed uniformly. Streamtube cross-sections (see Figure 3) are considered infinitely-far upstream (∞), shortly upstream (w^+), shortly downstream (w^-) and infinitely-far downstream (e) of the kite actuator annulus (w), such that stagnation pressure and angular momentum are conserved between ∞ and w^+, as well as w^- and e.

The normalized rotor area can be approximated as:

$$\frac{A_\mathrm{w}}{S} \approx \frac{\pi\left(\widetilde{z}c + \frac{1}{2}\not{R}c\right)^2 - \pi\left(\widetilde{z}c - \frac{1}{2}\not{R}c\right)^2}{S} \approx 2\pi\widetilde{z}. \tag{25}$$

Assuming that there is no axial change in velocity between w^+ and w^-, and that the pressure at e has recovered to

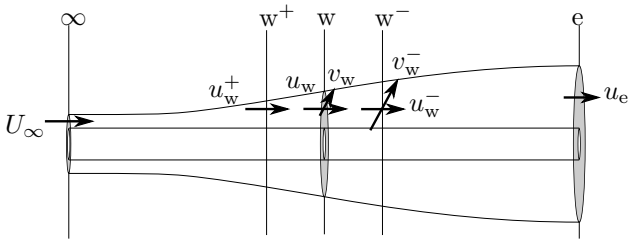

Fig. 3. A sketch of relevant streamtube cross-sections, with streamtube expansion exaggerated for visibility.

the original free-stream pressure, the pressure difference across the kite actuator annulus can be found:

$$p_\mathrm{w}^+ - p_\mathrm{w}^- = \tfrac{1}{2}\rho U_\infty^2 4(a - a^2). \tag{26}$$

This pressure difference causes a thrust across the annulus:

$$\widetilde{T} = \frac{T}{q_\infty S} = \frac{A_\mathrm{w}}{S}\frac{\left(p_\mathrm{w}^+ - p_\mathrm{w}^-\right)}{q_\infty} = 8\pi(a - a^2)\widetilde{z}. \tag{27}$$

It is assumed that there is a linear increase in angular velocity between w^+ (where the angular velocity is zero) and w^-. This corresponds to a tangential velocity $v_\mathrm{w}^+ = 0$, $v_\mathrm{w} = a'\lambda U_\infty$, and $v_\mathrm{w}^- = 2a'\lambda U_\infty$. Considering streamtube expansion, and the fact that $0 \leq a' \leq 1$, it is assumed that the tangential velocity infinitely far downstream is negligible. Then, the following holds:

$$\widetilde{Q} = \frac{\rho_\mathrm{air} u_\mathrm{w} A_\mathrm{w}\ v_\mathrm{w}^-\ \widetilde{z}c}{q_\infty S c} = 8\pi(1 - a)a'\lambda\widetilde{z}^2. \tag{28}$$

With the thrust and torque expressions from the blade-element perspective and the momentum perspective, it remains to state the combined expressions that implicitly determine the induction.

3.3 Combined Blade-Element Momentum Expressions

The BEM expressions for thrust and torque allow the inclusion of induction into the aerodynamic model in various degrees, allowing the model to easily switch between the NI, AI, and AA cases.

In the NI case, the axial induction factor is known:

$$a = 0. \tag{29}$$

Otherwise, the axial induction factor must implicitly equate the blade-element thrust (20) to the momentum thrust (27), without allowing the flow to reverse:

$$N\widetilde{\mathbf{F}}\cdot\hat{\boldsymbol{x}} - 8\pi(a - a^2)\widetilde{z} = 0, \tag{30}$$

$$0 \leq a \leq 0.5. \tag{31}$$

Similarly, in the NI and AI cases, the angular induction factor is known:

$$a' = 0. \tag{32}$$

Otherwise, the angular induction factor is determined implicitly by equating the blade-element torque (23) to the momentum torque (28), while considering the sign of the angular induction in (6):

$$N\left(\widetilde{\mathbf{Q}}_{\mathrm{k}}+\widetilde{\mathbf{Q}}_{T_D}\right)\cdot(-\hat{\boldsymbol{x}})-8\pi(1-a)a'\lambda\widetilde{z}^2=0, \quad (33)$$

$$0\leq a'\leq 1. \quad (34)$$

Using the model described until this point, we can formulate an optimization problem to estimate the effect of including induction on MAWES designs.

4. OPTIMAL DESIGN PROBLEM

Defining the optimization variable $\boldsymbol{W}\in\mathbb{R}^{19}$ that contains the variables $[\mathbf{R},\widetilde{x},\widetilde{z},\lambda,\widetilde{\phi},f,a,a',\xi,\zeta,\kappa]^T$, the question under consideration is whether the solution to the NI power optimization problem:

$$\min_{\boldsymbol{W}} \quad -\widetilde{P} \quad (35a)$$
$$\text{st.} \quad (29),\text{ and }(32) \quad (35b)$$
$$(1),(9),(10),(11),(21),\text{ and }(22) \quad (35c)$$
$$0\leq f\leq 1.0,\text{ and }\widetilde{x},\widetilde{z},\widetilde{\phi}>0, \quad (35d)$$

is significantly different from the solution to the AI power optimization problem:

$$\min_{\boldsymbol{W}} \quad -\widetilde{P} \quad (36a)$$
$$\text{st.} \quad (30),(31),\text{ and }(32) \quad (36b)$$
$$(35c),\text{ and }(35d), \quad (36c)$$

and the solution to the AA power optimization problem:

$$\min_{\boldsymbol{W}} \quad -\widetilde{P} \quad (37a)$$
$$\text{st.} \quad (30),(31),(33),\text{ and }(34) \quad (37b)$$
$$(35c),\text{ and }(35d). \quad (37c)$$

The optimization problem is posed in the symbolic language CasADi (Andersson et al., 2012) and solved with the interior point solver Ipopt (Wächter and Biegler, 2006).

This optimization problem can be considered with values that describe a reasonable rigid-wing, lift-mode AWES at 400m altitude(Ruiterkamp and Sieberling, 2014): $\widetilde{m}=1.4397$, $\mathcal{R}=10.0$, $\widetilde{\sigma}_T=2.1196\cdot10^6$, and $\widetilde{\rho}_T=822.9572$. Normalization values correspond to a generalized atmospheric model suggested for AWE purposes (Archer, 2014) and a Dyneema tether (Bosman et al., 2014) with a tolerable tether stress that is conservatively chosen as one-fifth of the 10 percent mean breaking load, as AWE tethers are safety-critical components for whom fatigue is not yet well understood.

5. RESULTS AND DISCUSSION

The obtained solutions (see Figures 4 and 5) are possibly only local minima, but appear close to Loyd's theoretical limit (Loyd, 1980) with an NI reel-out factor (0.3758 for $N=2$) close to 1/3. The trends described here are also found when the fixed parameters ($\widetilde{m}$, $\mathcal{R}$, $\widetilde{\sigma}_T$, and $\widetilde{\rho}_T$) correspond to other rigid AWE kites, like those considered by Vander Lind (2014) and Zanon et al. (2014).

When axial induction is modelled, the axial induction factor a is within the range where BEM is applicable, and is not negligibly small. Further, AI and AA cases generate significantly less power than NI cases. As a comparison, when a MAWES with two 3m^2-kites flies in a freestream of velocity $U_\infty=10$m/s and air density $\rho_{\mathrm{air}}=1.1786$kg/m^3,

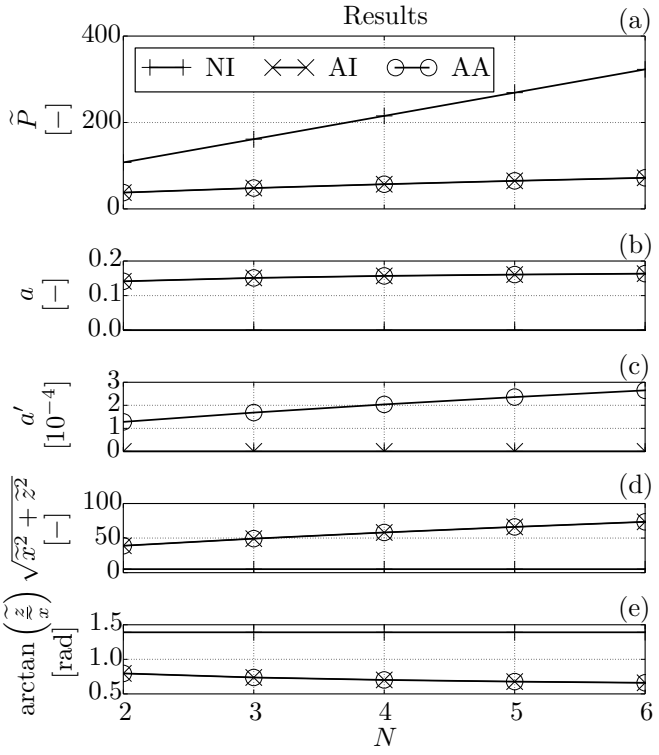

Fig. 4. Results vs. induction and number of kites: (a) non-dimensional power, (b) axial induction factor, (c) angular induction factor, (d) tether-length, and (e) tether-angle.

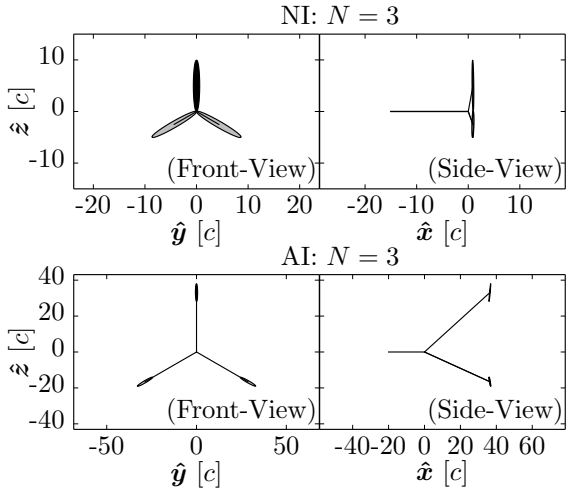

Fig. 5. Sample of position results: top kite-and-secondary-tether is analyzed; others are symmetrically repeated.

the AA case predicts 67kW pulling power, and the NI case predicts 190kW.

Increasing the number of kites in the AI and AA cases increases the interference between the kites and the flow, but acts purely as a force multiplier in the NI cases, such that differences between NI cases and AI and AA cases increase with the number of kites.

There appears to be very little difference in the results of the AI and AA cases, suggesting that angular induction is not necessary in MAWES modelling. This is reasonable as MAWES maximize their power production when the

torque on the system is close to zero, for a consistently high rotational velocity. Indeed, the angular induction factors found in the AA case are very small, though the lower bound of (34) remains inactive.

The AoA bound (10) is always saturated at $\alpha = 0.209$ radians, far from the maximum elliptical wing lift-to-drag AoA ($\alpha_{L/D_{\max}} = 0.0339$ radians for $C_{D_0} = 0.10$ and $\mathit{Æ} = 10$). As Loyd's theoretical limit (Loyd, 1980) for power proposes maximizing the system C_L^3/C_D^2 and the secondary tether drag is non-negligible, the kite lift must be maximized.

The kite location causes a three-way trade-off in the available power. First, long tether-lengths decreasing the effect of induction as each kite is further from the other kites' trailing vortices. Second, small angles between the secondary tether and the rotation axis increase the available power by allowing a greater portion of the resultant force to contribute to the power generation. Third, short tether-lengths increase the power by decreasing tether-drag. In the NI case, there is no induction, and the tether-drag effect is much stronger than the vector-projection effect. Consequently, the no-collision constraint (1) is active. In comparison, the AI and AA cases find moderate secondary tether lengths, with kites that are further downwind of the tether-connection point.

A larger kite centrifugal force will allow the MAWES to support a larger radius of rotation. Consequently, optimal kites in AI and AA cases are heavier than those in NI cases, as seen in Figure 6. That is, MAWES designed for NI tend to have short secondary tethers, and lightweight kites, as in a hub- and root-less wind turbine. In contrast, MAWES designed for AI or AA have longer secondary tethers and heavier kites.

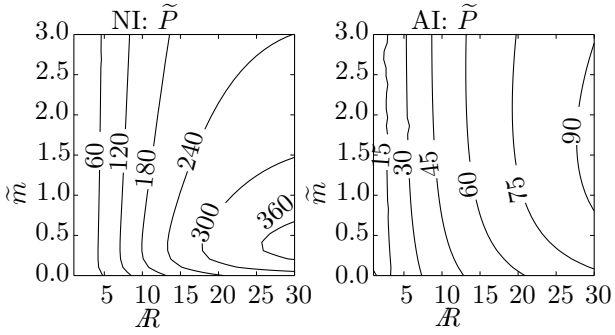

Fig. 6. Non-dimensional power vs. mass ratio and aspect ratio, for NI and AI, $N = 3$

Whereas the NI results are not consistent with the modelling assumptions, due to the short secondary tethers, the AI results do appear consistent with the assumptions and resemble an imagined MAWES. The validity of these modelling assumptions, particularly the rotational symmetry of the system due to the neglected gravity and main tether, is the subject of an ongoing analysis. As Figure 4 (top) resembles comparable plots (Manwell et al., 2009) for wind turbines, and Zanon et al. (2014) predicts only half the two-kite induction power loss as found in this analysis, an asymmetric MAWES study appears to be justified.

6. CONCLUSION

In the power optimization of a MAWES, including axial induction leads to a significantly different system performance and design-point: a power decrease of approximately 60 percent and designs with heavier kites and longer secondary tethers. Given the assumptions made in this study, axial induction is highly relevant to MAWES optimal design and control, while angular induction is negligible.

REFERENCES

Andersson, J., Åkesson, J., and Diehl, M. (2012). CasADi: A Symbolic package for automatic differentiation and optimal control. 297–307. Springer Berlin Heidelberg.

Archer, C.L. (2014). An Introduction to meteorology for airborne wind energy. In U. Ahrens, M. Diehl, and R. Schmehl (eds.), *Airborne Wind Energy*, chapter 6, 81–94. Springer, Heidelberg, Germany.

Bosman, R., Reid, V., Vlasblom, M., and Smeets, P. (2014). Airborne wind energy tethers with high-modulus polyethylene fibers. In U. Ahrens, M. Diehl, and R. Schmehl (eds.), *Airborne Wind Energy*, chapter 33, 563–586. Springer, Heidelberg, Germany.

Houska, B. and Diehl, M. (2007). Optimal control for power generating kites. In *Proc European Control Conference*, 1–14.

Jacobs, E.N. and Sherman, A. (1937). Airfoil section characterists as affected by variations of the reynolds number. Technical report, National Advisory Committee for Aeronautics. NACA-TR-586, Langley Field, Virgina, USA.

Loyd, M.L. (1980). Crosswind kite power. *Journal of Energy*, 4(3), 106–111.

Manwell, J.F., McGowan, J.G., and Rogers, A.L. (2009). *Wind energy explained: Theory, design and application*. Wiley, Chippenham, Wiltshire, UK, 2 edition.

Ruiterkamp, R. and Sieberling, S. (2014). Description and preliminary test results of a six degrees of freedom rigid wing pumping system. In U. Ahrens, M. Diehl, and R. Schmehl (eds.), *Airborne Wind Energy*, chapter 26, 443–458. Springer, Heidelberg, Germany.

Vander Lind, D. (2014). Analysis and flight test validation of high performance airborne wind turbines. In U. Ahrens, M. Diehl, and R. Schmehl (eds.), *Airborne Wind Energy*, chapter 28, 473–490. Springer, Heidelberg, Germany.

Von Mises, R. (1959). *Theory of flight*. Dover, New York, New York, USA, 2 edition.

Wächter, A. and Biegler, L. (2006). On the implementation of a primal-dual interior point filter line search algorithm for large-scale nonlinear programming. *Mathematical Programming*, 106(1), 25–57.

Zanon, M., Gros, S., Andersson, J., and Diehl, M. (2013). Airborne wind energy based on dual airfoils. *IEEE Transactions on Control Systems Technology*, 21(4), 1215–1222.

Zanon, M., Gros, S., Meyers, J., and Diehl, M. (2014). Airborne wind energy: Airfoil-airmass interaction. In *Proceedings of the 19th World Congress The International Federation of Automatic Control*. Cape Town, South Africa.